Journal of Applied Fluid Mechanics, Vol. 17, No. 11, pp. 2299-2312, 2024.
Available online at www.jafmonline.net, ISSN 1735-3572, EISSN 1735-3645.
https://doi.org/10.47176/jafm.17.11.2647

Automated Design Process of a Fixed Wing UAV Maximizing Endurance

M. Sahraoui[1], A. Boutemedjet[1], M. Mekadem[1†], and D. Scholz[2]

[1] *Laboratory of Fluid Mechanics, Ecole Militaire Polytechnique, Bordj El Bahri, 16046, Algiers, Algeria*
[2] *Aircraft Design and Systems Group (AERO), Hamburg University of Applied Sciences, Hamburg, 20099, Germany*

†*Corresponding Author Email: mahmoud.mekadem@emp.mdn.dz*

ABSTRACT

Unmanned aerial vehicle (UAV) design necessitates significant effort in prototyping, testing, and design iterations. To reduce design time and improve wing performance, an automated design and optimization framework is proposed utilizing open-source software, including OpenVSP: VSPAERO & Parasite Drag Tool, XFOIL, and Python. This study presents a preliminary UAV wing design methodology, emphasizing weight estimation, drag analysis, stall prediction, and endurance optimization. The maximum takeoff weight of the UAV was calculated after estimating the empty weight using a linear regression from data from 20 existing similar UAVs. The wing and engine sizing were determined using the matching plot technique. A solver with low-fidelity models, combining the Vortex Lattice Method (VLM) and analytical expressions, was used to predict the drag coefficient and maximum lift coefficient of the designed wing. An optimization process using a genetic algorithm was applied to maximize endurance while satisfying requirements such as rate of climb, stall, and maximum speeds. The optimized wing was analyzed with computational fluid dynamics (CFD), and its aerodynamic characteristics were compared with those obtained using VLM and the suggested aerodynamic solver. According to the CFD results, the proposed aerodynamic solver estimated the drag coefficient at zero angle of attack with an error of 17.2% compared to 63.1% using the VLM classic method. The error on the maximum lift coefficient estimation was limited to 5.3%. In terms of optimization, the framework showed an increase in the endurance ratio of up to 2% compared to the Artificial Neural Network method coupled with XFLR5. The primary advantage of the suggested framework is the utilization of open-source software, giving a cost-effective and accessible solution for small and medium-sized startups to design and optimize UAVs to achieve mission objectives.

Article History

Received February 6, 2024
Revised April 18, 2024
Accepted May 9, 2024
Available online September 1, 2024

Keywords:

UAVs design
Optimization framework
OpenVSP
XFOIL
Genetic algorithm
ANN-XFLR5

1. INTRODUCTION

The aircraft design is an iterative process. It goes through these three essential stages: conceptual, preliminary, and detailed design. The wing is a critical element of an aircraft, responsible for providing lift and supporting the weight of the plane. Hence, reducing the time of wing conception and optimization is vital to accelerate the aircraft development process. In recent years, numerical design process modeling has played a significant role in the design of UAVs. It refers to the utilization of mathematical models (Hoseinzadeh & Stephan Heyns, 2022) and computational simulations (Ostadhossein & Hoseinzadeh, 2024) to analyze the behaviors of a design process. Numerical modeling allows designers to assess the performance of UAVs in general and airfoils in particular (Hoseinzadeh et al., 2021). However, it is important to acknowledge that while numerical models are valuable, experimental tests remain the most reliable tool for obtaining certain information (Bahrami et al., 2019; Hoseinzadeh et al., 2020). The study of unmanned aerial vehicle (UAV) wing design and optimization has grown in significance in recent years. As a result, scientists have adopted a variety of methodologies

NOMENCLATURE

ACRONYMS AND ABBREVIATIONS

ANN	Artificial Neutral Network	MAC	Mean Aerodynamic Chord
AOA	Angle of Attack	MDO	Multidisciplinary Optimization
API	Application Programming Interface	MOPSO	Multiple Objective Particle Swarm Optimization
AVL	Athena Vortex Lattice	MOTSA	Multiple Objective Tabu Search Algorithm
CFD	Computational Fluid Dynamics	PSO	Particle Swarm Optimization
DATCOM	Data Compendium	RANS	Reynolds-Averaged Navier-Stokes
EMWET	Elham Modified Weight Estimation Technique	UAV	Unmanned Aerial Vehicle
GA	Genetic Algorithm	VLM	Vortex Lattice Method

Symbol

$\left(\frac{L}{D}\right)_{max}$	maximum glide ratio	a_1, a_2	coefficients in the drag polynomial equation
$\frac{C_{L,max}}{c_{lmax}}$	ratio between the maximum lift coefficient of the wing and the maximum lift coefficient of the section in the DATCOM method	$c_{l,i}$	ideal lift coefficient
$C_L^{\frac{3}{2}}/C_D$	endurance ratio	c_{lmax}	airfoil maximum lift coefficient
$V_{max}{}^*$	required maximum speed	$c_{l\alpha}$	airfoil lift curve slope
V_s^*	required stall speed	m_E	empty weight
C_D	drag coefficient	m_{TO}	maximum take-off weight
C_{D0}	parasite drag coefficient	m_p	Payload weight
C_{Dmin}	minimum drag coefficient	b	wing span
$C_{L,min\,Drag}$	lift coefficient value corresponding to the minimum drag coefficient	e_i	internal energy per unit of mass
$C_{L,VLM}$	lift coefficient corresponding to the angle of attack at which lift curve slope ceases to be linear	f	internal force per unit of mass
$C_{L,max}$	wing maximum lift coefficient	m	mass
C_L	lift coefficient	p	fluid pressure
C_{LR}	take-off rotation lift coefficient	q	heat transfer
$C_{L\alpha}$	wing lift curve slope	T	penalty term
C_f	skin friction coefficient	t	time
C_r	root chord	V	air flow velocity
C_t	tip chord	A	aspect ratio
E_{max}	maximum endurance ratio	FF	Factor Form
ROC^*	required rate of climb	L	UAV length
R_e	Reynold's number	$N - pop$	number of chromosomes in the population
S_{TO}	takeoff run distance	P	engine power
S_{ref}	reference area	P/m	power loading
S_{wet}	wetted area	Q	interference factor
V_{TO}	take-off speed	ROC	rate of climb
V_c	cruise speed	a, b, c	coefficients in the lift polynomial equation
V_{max}	maximum velocity	e	oswald factor
V_s	stall speed	g	gravity constant
W_l, m/S	wing loading	t/c	thickness-to-chord ratio

GREEK SYMBOLS

$\alpha_{C_{L,max}}$	angle of attack corresponding to the maximum lift coefficient	α	angle of attack
α_*	angle of attack at which lift curve slope ceases to be linear	μ	friction coefficient
α_0	zero lift angle of attack	σ	air density ratio
α_s	stall angle	∇	gradient operator
η_p	propeller efficiency	θ	twist angle
ρ_0	air density at sea level	λ	taper ratio
$\tilde{\upsilon}$	turbulent viscosity	ρ	air density
$\Delta C_{L,max}$	Mach number correction	τ	tensor of viscosity
$\Delta\alpha_{C_{L,max}}$	angle of attack increment	φ	sweep angle

to improve the design of UAV wings for diverse uses. A commonly used approach is Computational Fluid Dynamics (CFD) simulations. In a study by Kapsalis et al. (2021), the Taguchi technique and CFD were coupled using the Ansys CFX software. The objective functions of the study were top speed, takeoff runway length, and gross takeoff weight; the design parameters were aspect ratio (A), taper ratio (λ), and sweep angle (φ).

The performance of UAV wings can be predicted using machine learning approaches like neural networks (Sun & Wang, 2019). This approach to airfoil design optimization has been the subject of several investigations. For example, (Haryanto et al., 2014) maximized the lift-to-drag ratio using a combination of Artificial Neural Networks (ANN) and Genetic Algorithm (GA). Du et al. (2021 presented an interactive framework based on a neural network to optimize airfoil shapes for both subsonic and transonic regimes. This framework takes Reynolds number, Mach number, angle of attack, and airfoil geometry as inputs, with target lift and thickness as constraints, and minimizes drag coefficient as the objective. Boutemedjet et al. (2019) also employed a combined GA-ANN approach to optimize UAV wing design during the preliminary stage. Their focus was maximizing the endurance ratio and minimizing the drag coefficient. They used XFLR5 for numerical simulations to generate the training data for the neural network. Azabi et al. (2019) present a multi-objective optimization framework (ANN-MOPSO-AVL) that couples an ANN trained using AVL software with a Particle Swarm Optimization (PSO) process. The framework is deployed to optimize the shape of a U-tailed UAV. Two objective functions were included: maximizing flight endurance and minimizing the UAV mass. A comparison of Pareto front solutions obtained using ANN-MOPSO, MOTS (Multiple Objective Tabu Search Algorithm), and MOPSO with a U-tailed UAV demonstrates the potential power of ANNs when used to solve this type of design challenge, in terms of both computation time reduction and the number of valid solutions.

Over the past few decades, with the advent of new technologies, there has been a surge in interest in Multidisciplinary Design Optimization (MDO). Benaouali and Kachel (2019) developed an MDO framework which integrates geometric modeling in Siemens NX (2024), aerodynamic meshing in ICEM CFD, flow solution using Ansys Fluent, structural finite element modeling in MSC Patran (2024), and structural sizing in MSC Nastran (2024) to achieve a maximum range while maintaining lift coefficient and structure safety. In the same context, Masood and Wei (2018) focused on MDO for the wing of subsonic aircraft. They aimed to maximize wing performance by considering three disciplines: structure (weight), aerodynamics (L/D ratio), and flight performances (endurance and range). XFOIL software (2024) was used for aerodynamic analysis, while the weight of the wing was estimated using a semi-empirical equation of HOWE. Their design study contained ten variables, and a GA was applied to search for the best configuration. Elham and Van Tooren (2014) also developed an optimization framework to find the Pareto front for a winglet with minimum drag and weight. In this work, a quasi-3D aerodynamic solver was proposed and validated with the high-fidelity solver. For weight estimation, they proposed a quasi-analytical method called the Elham Modified Weight Estimation Technique (EMWET).

Among the common challenges facing the design process are the time-consuming nature of design iterations and the high cost of simulation. Therefore, this paper focuses on automating the preliminary design of a mini electric UAV to enhance wing planform aerodynamics and flight performance. This work addresses the challenge of conceptualizing a UAV design framework, called OpenVSP-API, that utilizes OpenVSP (2024) (VSPAERO & Parasite Drag Tool) and XFOIL with a highly interoperable Python Application Programming Interface (API). This framework allows designers to perform calculations during the preliminary design phase with good fidelity in a short time.

The remainder of the paper is organized as follows: Section 1 will present a concise overview of the methodology employed in UAV design. Section 2 describes the study framework, Section 3 outlines the UAV conceptual design, Section 4 explains the proposed aerodynamic solver, Section 5 presents the validation of the framework's performance, Section 6 details the CFD analysis for the optimal wing, and Section 7 provides the conclusions.

2. OPENVSP- API FRAMEWORK DESCRIPTION

OpenVSP can be integrated with Python through an API written virtually in C++. A script carries out this integration. In the beginning, the Python 3.8 version was installed via Anaconda. Then, environments named ‘vsppytools’ in OpenVSP 3.25.0 should be created and activated. It should be noted that the Python version used to compile OpenVSP must match. It’s known that OpenVSP uses VSPAERO for the aerodynamic analysis; this solver is based on the VLM method (Hedman, 1966). The viscous drag is estimated using the Parasite Drag Tool and XFOIL for the lift correction, as will be described in the next section. Figure 1 represents the framework environment.

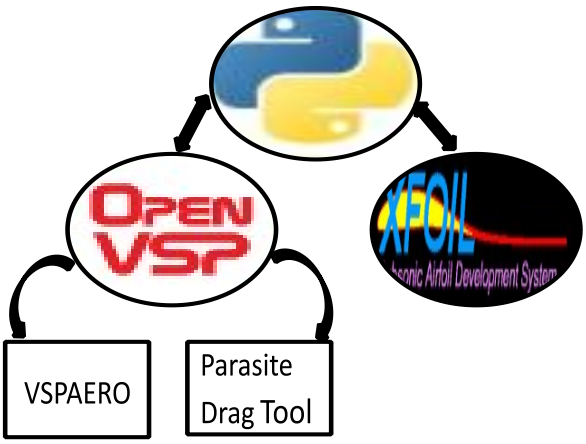

Fig. 1 Framework environment

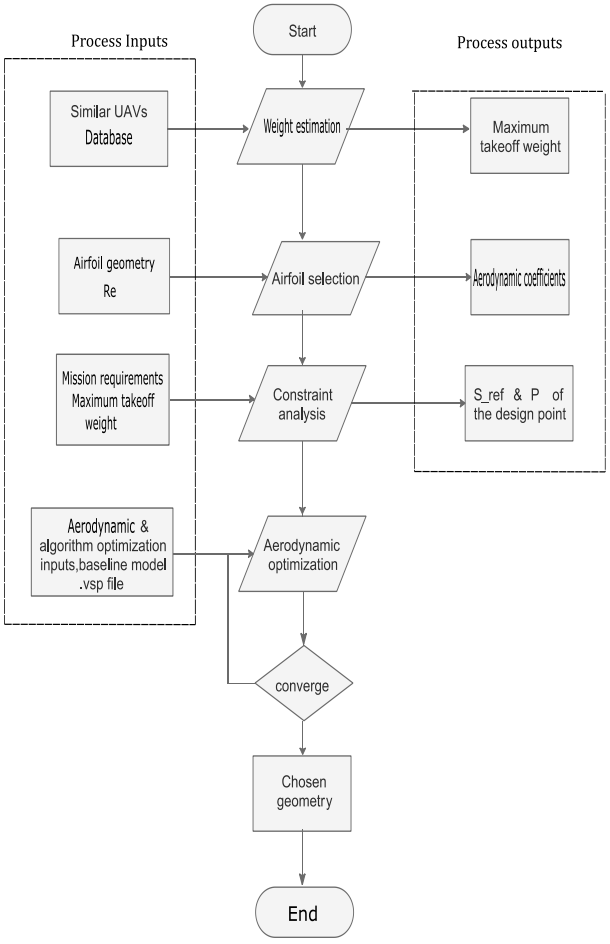

Fig. 2 General architecture of the framework

The proposed process, illustrated in Fig. 2, begins by collecting data through market analysis of similar UAVs. This data is used during take-off weight estimation. The design point is then determined through constraint analysis. Following the selection of an adequate airfoil, wing design parameters are obtained using a single-objective aerodynamic optimization with a genetic algorithm, while respecting all constraints and requirements.

3. PRELIMINARY DESIGN

Following the selection of the UAV configuration comes a critical step: the preliminary design. During this phase, three essential parameters were calculated: maximum take-off weight (m_{TO}), reference area (S_{ref}), and engine power (P). An outline of the preliminary design for the UAV is provided in the parts that follow.

3.1 Mission Requirements

To accomplish the surveillance mission depicted in Fig. 3 at an altitude of 300 m above sea level, a mini-drone has been designed. The UAV has a maximum speed of 100 km/h and a stall speed of 10 m/s. The propeller is powered by an electric powerplant due to its low operating costs. Furthermore, the UAV requires maximum endurance. Table 1 shows the design requirements.

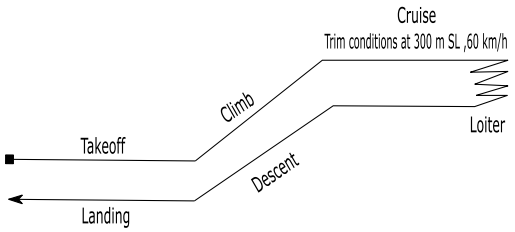

Fig. 3 UAV flight mission

Table 1 UAV specifications

Maximum take-off weight (m_{TO})	≤ 10 kg
Payload weight (m_p)	1.5 kg
Stall speed	10 m/s
Maximum speed	100 km/h
Cruise speed	60 km/h
Endurance	60 min
Radius	60 km
Rate of climb	2.5 m/s … 5 m/s
Altitude	300 m (SL)
Equipment	Camera, battery, avionic, parachute
Engine	Electric motor

3.2 Weight Estimation

The following equation provides the maximum takeoff weight:

$$m_{TO} = m_p + m_E \quad (1)$$

The payload, which includes the necessary electronics for the camera and the parachute, does not exceed 1.5 kg.

During an early phase of electric UAV design, it is necessary to point out that the structure, engine mass, propeller, batteries, fixed equipment, and anything else not deemed to be a payload were all included in the empty weight. It was estimated using a linear regression of data from 20 existing UAVs collected from the following sources: (Air Force Technology | Air Defence News & Views Updated Daily, 2024), (Gallet, n.d.), (Military Factory - Global Defense Reference, n.d.), and (GlobalSecurity, n.d.), as shown in Table 2. Figure 4 displays the static data of m_E versus the m_{TO}. The resulting linear fit equation is:

$$m_E = 0.848\, m_{TO} - 0.334 \quad (2)$$

By combining Eq. (1) and (2), the empty weight and the total weight were estimated to be 6.17 kg and 7.67 kg, respectively.

3.3 Matching Plot Technique

This section is very important for wing and engine sizing. The design point's wing loading (m/S) and power loading (P/m) are calculated using a matching plot approach. The following list of equations was used for the diagram construction (Sadraey, 2013):

Table 2 Similar UAV's database

	m_{TO}(kg)	m_E(kg)	m_p(kg)	b(m)	L (m)	V_{max}(km /h)	Endurance (h)	Altitude (m)
Utva Vrabac	7	5.5	1.5	2.8		85	0.67	300-500
Bayraktar Mini UAV	5	3.5	1.5	2	1.2	55	0.67	915
WB Electronics Warmate	6.7	5.3	1.4	1.6	1.1	80	≤ 1.17	500
Puma LE	12.2	9.7	2.5	4.6	2.2	76	6.5	3048
Puma 3 AE	7	5.2	1.8	2.8	1.4	83	2	3048
Thalys SpyRanger	14	12.8	1.2	3.9		90	2.5	4500
Dragonfish Pro	17	14.5	2.5	3.04	1.65	108	3	6000
Dragonfish Standard	9	7.5	1.5	2.3	1.29	108	2	6000
Dragonfish Lite	5.5	4.5	1	1.6	0.97	108	1.25	4000
ALTIUS-600	12.25	9.08	3.17	2.54	1	167	4	
BlueBird SpyLite	9	7.7	1.3	2.7	1.35	120	4	1000
BlueBird Thunder B	28	24.5	3.5	4	1.9	137	24	4877
Silver Fox	13	10.8	2.2	2.4	1.45	93	10	3657
Vector	8	7	1	2.8	1.63	85	2	
Spaitech ARDEA	10	8	2	3.2		120	2.5	2500
Orlan-10	16.5	12.5	4	3.1	2	150	≈ 18	≤ 5000
Lockheed Stalker	8	7	1	3		80	2	4572
Skyeton Raybird-3	20	15	5	3	1.83	160		3100
Leleka-100	6	5.1	0.9	1.98	1.13	100	≤ 2.5	1500
Yagua	12	10	2	2.5	2	100		4100

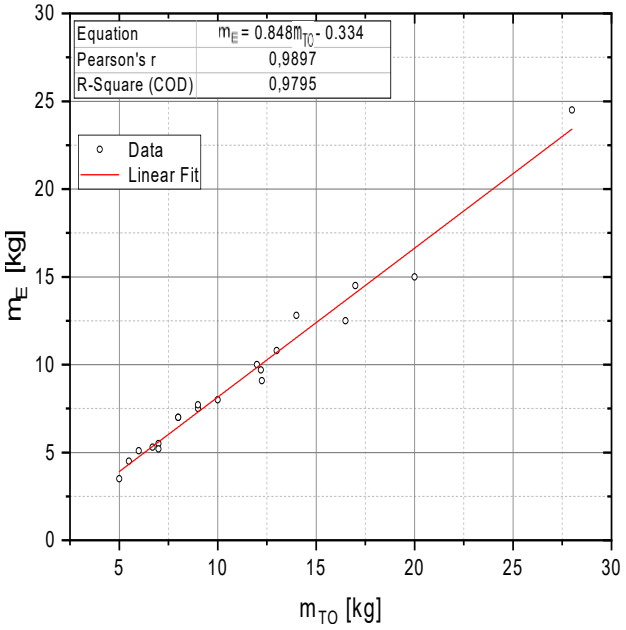

Fig. 4 m_E vs. m_{TO} of existing UAVs

- Stall:

$$\frac{m}{S} = \frac{1}{2g} \cdot \rho \, {V_s}^2 \, C_{L,max} \tag{3}$$

- Maximum speed:

$$\frac{P}{m} = \frac{1}{2\eta_p} \, \rho_0 {V_{max}}^3 C_{D0} \, \frac{1}{\frac{m}{S}} + \frac{2 \, K \, g^2}{\eta_p \, \rho \, \sigma \, V_{max}} \, \frac{m}{S} \tag{4}$$

- Rate of climb:

$$\frac{P}{m} = g \left(\frac{ROC}{\eta_p} + \sqrt{\frac{2 \, g}{\rho \sqrt{\frac{3 C_{D0}}{K}}}} \, \frac{m}{S} \left(\frac{1.115}{\left(\frac{L}{D}\right)_{max} \eta_p} \right) \right) \tag{5}$$

- Takeoff run:

$$\frac{P}{m} = g \frac{\mu - \left(\mu + \frac{C_{DG}}{C_{LR}}\right) exp\left(0.6 \, \rho \, C_{DG} \, S_{TO} \, \frac{1}{\frac{m}{S}}\right)}{1 - exp\left(0.6 \, \rho \, C_{DG} \, S_{TO} \, \frac{1}{\frac{m}{S}}\right)} \frac{V_{TO}}{\eta_p} \tag{6}$$

Here: g = 9.81 $m^2 \cdot s^{-1}$, $C_{L,max}$= 1.45, ρ = 1.19 kg/m^3, ρ_0 = 1.225 kg/m^3, $\sigma = \rho/\rho_0$, η_p= 0.7, C_{D0}= 0.035

$K = 1/(\pi \, e \, A)$, $(L/D)_{max}$ = 12, A = 10. The design also considers a required takeoff run (S_{TO}) of 150 m. The friction coefficient (μ) is set to 0.04. C_{DG} and C_{LR} are calculated to be 0.18 and 1.22, respectively. It is noticed that the previous parameters were determined across a conceptual computation considering the type of mission

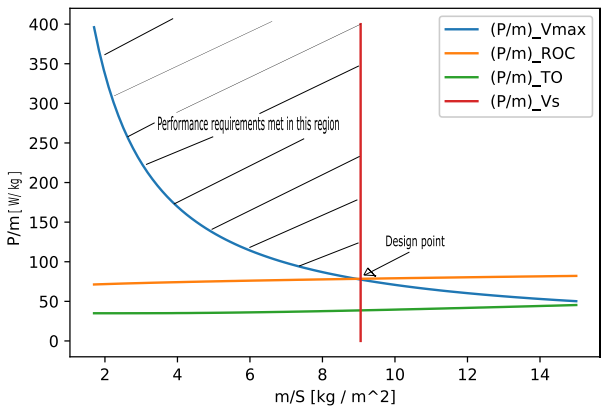

Fig. 5 Matching plot diagram

and the required performances. Fig. 5 illustrates the matching plot technique described in this subsection.

The design point's coordinates are thus determined to be m/S = 9.05 kg/m^2 and P/m = 82.7 W/kg. This translates to a reference area of 0.847 m^2, and an engine power of 635 W.

3.4 Airfoil Choice

Once the reference surface (S) is obtained, the wing profile required to support a mass of 7.67 kg is selected. We then determine the ideal lift coefficient for the profile.

It was taken as the value that corresponds to the minimum drag. It was calculated using the following equation (Sadraey, 2013):

$$c_{l,i} = \frac{2mg}{0.855 \cdot \rho \cdot {V_c}^2 \cdot S} = 0.66 \quad (7)$$

The airfoil "SD7062" is widely used in RC planes with a low Reynolds number (Traub, 2013; Boutemedjet et al., 2019) because it offers a good lift-to-drag ratio and a gentle post stall (Anılır & Kurtuluş, 2023; Hutagalung et al, 2016). This airfoil, with a thickness of 14%, enables effective structural reinforcement. It was simulated for Reynolds numbers of $1.93 \cdot 10^5, 3.22 \cdot 10^5$, and $5.37 \cdot 10^5$, which correspond to stall, cruise, and maximum velocity, respectively. As shown in Fig. 6, the SD7062 airfoil exhibits a lift coefficient close to the ideal value identified earlier, making it a suitable choice for achieving the optimized wing shape.

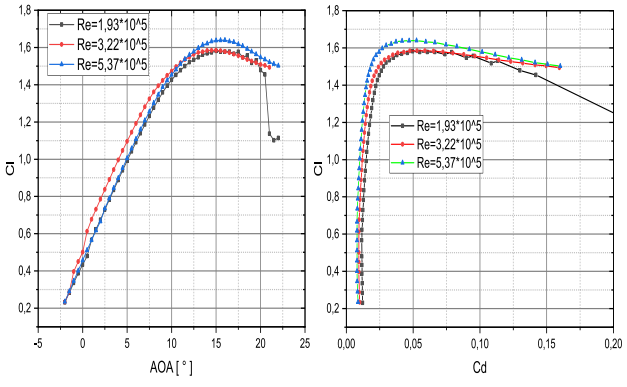

Fig. 6 SD7062 Airfoil: Lift and Drag Coefficients

4. AERODYNAMIC SOLVER

The evaluation of aerodynamic coefficients is an important part of aircraft design, and the choice of an aerodynamic solver is critical. The aim here is to work with an efficient solver that gives results close to CFD.

The Vortex Lattice Method (VLM), a numerical approach introduced by Falkner (1943), simulates fluid behavior by representing it with a series of vortices. It's a linear solution method based on ideal flow theory. VLM has a good estimation of the lift curve slope, induced drag, and force distribution at low angles of attack, although it considers the flows as an incompressible and inviscid fluid, where the thickness effect and viscosity are neglected. In addition, it cannot predict the stall phenomenon. To address this limitation, several modifications were proposed for implementation in our house code. This new approach, described below, is able to predict the nonlinear effects of viscosity on both the stall region and parasite drag, resulting a good estimation design point (m/S, P/m).

The results were validated by referencing CFD results for the isolated wing presented in Fig. 7 and its dimensions, as provided in Table 3 (Boutemedjet et al., 2019).

4.1 Drag Estimation

C_D calculation is an essential task during UAV performance evaluation. The effects of an imprecise drag estimate cannot be overly predictable, as either an overly optimistic or overly pessimistic drag estimate will result in a design with an inefficient allocation of fuel volume and engine size.

The total aircraft drag coefficient consists of a lift-independent component, C_{Dmin}, and another component

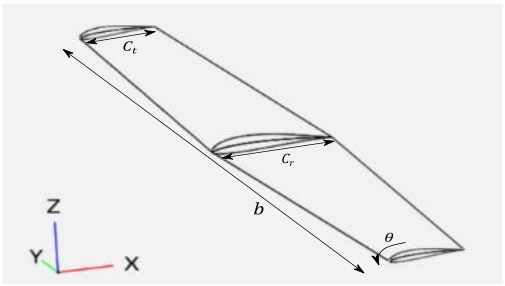

Fig. 7 Isolated wing in OpenVSP

Table 3 Geometric dimensions of the studied wing

Parameters	Value
b [m]	2.818
C_t [m]	0.330
C_r [m]	0.206
MAC [m]	0.268
S_{ref} [m^2]	0.755
λ	0.62
A	10.51
θ [°]	-2

dependent on the lift produced by the vorticity shed into the wake, C_{Di}. Equation (8) (Anderson, 2016) provides the following expression:

$$C_D = C_{Dmin} + k\left(C_L - C_{L,min\,Drag}\right)^2 \quad (8)$$

The minimum drag coefficient ($C_{D,min}$) results from the combined effects of parasite drag (C_{D0}), compressibility drag, and drag due to excrescences, imperfections, and surface roughness. $C_{L,min\,Drag}$ is the lift coefficient value corresponding to the minimum drag coefficient C_{Dmin}. In this study, the focus is only on the consideration of parasite drag, which is a combination of friction and form drag.

The VLM code implemented in the VSPAERO solver can accurately estimate lift and induced drag; however, it cannot predict viscous effects, which leads to an underestimation of the drag. The proposed approach for rectifying CD involves expressing it in terms of CL as follows:

$$C_D = C_{D0} + a_1\, C_L + a_2\, {C_L}^2 \quad (9)$$

Where C_{D0} represents the zero-lift drag coefficient, or parasite drag, it's equal to the total drag coefficient where the lift coefficient is equal to zero. It is calculated by integrating a "Parasite Drag analysis" into the framework.

In general, the zero-lift drag coefficient is expressed by the following equation (Gudmundsson, 2013):

$$C_{D0} = C_f \cdot FF \cdot \mathrm{Q}\left(\frac{S_{wet}}{S_{ref}}\right) \quad (10)$$

Where: Q is the interference factor; it was taken 1. S_{ref} is the reference area, S_{wet} represents the corresponding wetted area, and it is given by (Gudmundsson, 2013): $S_{wet} = 2\,S \cdot k_b$, where k_b is equal to 1.07.

C_f is the skin friction coefficient for an equivalent flat plate. For a laminar flow, It's determined by the (Blasius, 1950) equation as:

$$C_f(laminar) = \frac{1.327}{\sqrt{R_e}} \quad (11)$$

For a turbulent flow ($R_e < 10^9$), an empirical correlation provided by (Schlichting & Kestin, 1961) has been selected:

$$C_f(turbulent) = \frac{0.455}{\log\,(R_e)^{2.58}} \quad (12)$$

A previous study (Pritchard & Mitchell, 2016) shows that equation 12 fits well with the experimental data.

FF is the corresponding form factor. It signifies drag rectification due to thickness and pressure drag. There are many empirical correlation methods implemented in the Parasite Drag Tool, such as EDET, Hoerner (Cheeseman, 1976), Torenbeek, DATCOM (Hoak & Carlson 1978) and (Covert, 1985). We chose to use Hoerner's method due to its excellent performance for small unmanned aerial vehicles operating at low subcritical Reynolds numbers. Also, it gives results very close to those of the CFD in the case of an isolated wing. The Hoerner's equation for ff wing estimation (with the maximum thickness located near or at 0.30 of the chord) is given by:

$$FF = 1 + 2(t/c) + 60(t/c)^4 \quad (13)$$

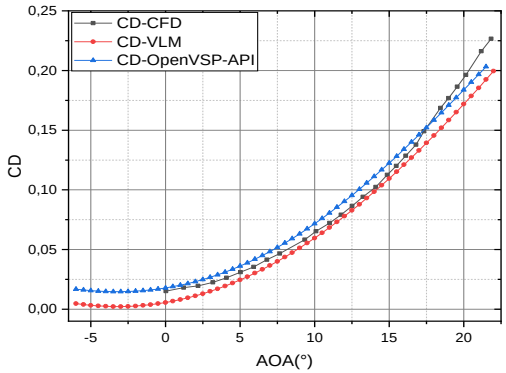

Fig. 8 Wing drag coefficient comparison

The results of the VLM code combined with the Parasite Drag tool are validated with the CFD results of an isolated wing in the reference study. It's noted that the flow conditions were calculated at an altitude of 300 m above sea level, using "US Standard Atmosphere 1976". In this investigation, the air density was determined to be 1.19 kg/m^3, with a dynamic viscosity of $1.17 \cdot 10^{-5} kg/m/s$ and a Reynolds number per unit length of $1.137 \cdot 10^6\ m^{-1}$. It was calculated on the mean aerodynamic chord. The validation of the C_D estimation implemented in the study code is shown in Fig. 8.

The drag coefficient of the isolated wing represented in Fig. 8 shows a good approximation that fits well with the CFD result. C_D at zero angle of attack was estimated to be 0.017, which is close to the value calculated by CFD (0.015), as compared to 0.006 calculated by the VLM method. This new approach results in a 17.2% error in the drag coefficient at a zero angle of attack, compared to the traditional VLM method's 63.1% error. As a result, a reduction of 45.9% in the absolute error of the drag coefficient has been achieved. The study framework's incorporation of viscous drag prediction explains this improvement. Furthermore, the study framework slightly overestimates the drag coefficient at the trim condition compared to the results from computational fluid dynamics (CFD). This overestimation could be beneficial for engine sizing purposes, as it allows for the selection of a slightly more powerful engine.

4.2 Lift Coefficient Correction

Despite having a high calculation strength for a low angle of attack and a fast convergence speed, VLM is unpredictable in stalls and post-stalls. There is a lot of research about the correction of the VLM method. One notable example is VLM-K (dos Santos & Marques, 2018), which is a correction based on the KIRCHOFF flow approach to nonlinear lift.

This paper proposes an alternative method for correcting VLM results. The framework implements this method as follows:

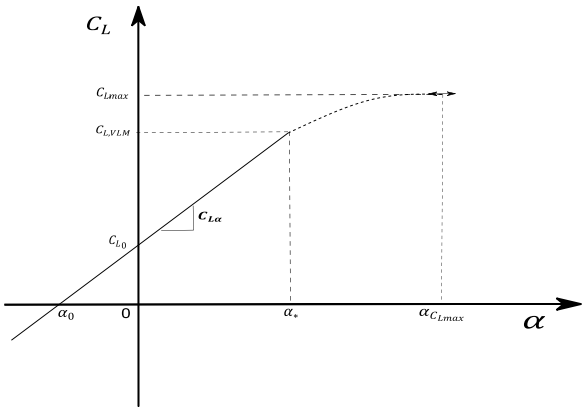

Fig. 9 Illustration graph of the method used

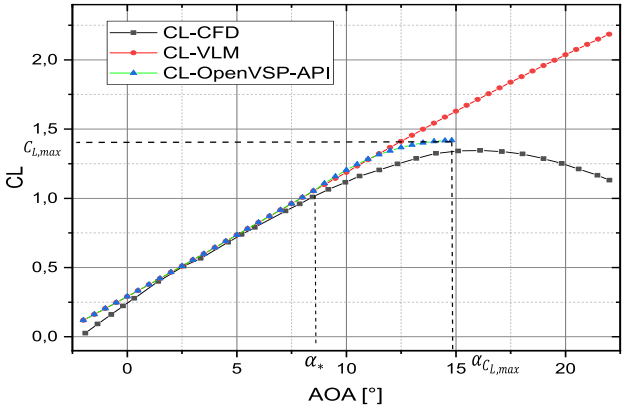

Fig. 10 Wing lift coefficient comparison

- For a linear zone where ($AOA \leq \alpha_*$) (see Fig. 9), the lift coefficient is taken from the VLM result. Where α_* represents the angle of appearance of the flow separation effects in the profile. It's taken as the angle when the absolute error between the airfoil lift coefficient and its tangent line at zero AOA exceeds 5%.
- For the nonlinear zone where: ($AOA \geq \alpha_*$), after getting the couple ($C_{L,max}, \alpha_{C_{L,max}}$), a polynomial interpolation is done in the following way:

$$C_L(\alpha) = a \cdot \alpha^2 + b \cdot \alpha + c \quad (14)$$

$$C_{L_\alpha} = 2a\alpha + b \quad (15)$$

The boundary conditions are applied to α_* and $\alpha_{C_{L,max}}$:

Where: $\alpha = \alpha_*$ the equation: $C_{L,VLM} = a \cdot {\alpha_*}^2 + b \cdot \alpha_* + c$ is satisfied.

While in: $\alpha = \alpha_{C_{L,max}}$, we have:

$$\begin{cases} 0 = 2a\,\alpha_{C_{L,max}} + b \\ C_{L,max} = a \cdot {\alpha_{C_{L,max}}}^2 + b \cdot \alpha_{C_{L,max}} + c \end{cases}$$

The final polynomial coefficients (a, b, and c) represented in Eq. (14) are:

$$\begin{cases} a = -\frac{C_{L,max} - C_{L,VLM}}{\left(\alpha_{C_{L,max}} - \alpha_*\right)^2} \\ b = -2a\alpha_{C_{L,max}} \\ c = C_{L,max} - b \cdot \alpha_{C_{L,max}} - a \cdot {\alpha_{C_{L,max}}}^2 \end{cases}$$

To estimate ($C_{L,max}, \alpha_{C_{L,max}}$) based on the DATCOM (Hoak & Carlson, 1978) Eq. (16) and Eq. (17), Mention that those equations are available for both incompressible and compressible flow.

$$C_{L,max} = \left(\frac{C_{L,max}}{c_{lmax}}\right) \boldsymbol{c_{lmax}} + \Delta C_{L,max} \quad (16)$$

$$\alpha_{C_{L,max}} = \frac{C_{L,max}}{\boldsymbol{C_{L\alpha}}} + \boldsymbol{\alpha_0} + \Delta\alpha_{C_{L,max}} \quad (17)$$

Where: ΔC_{Lmax} and $\Delta\alpha_{C_{Lmax}}$: are the Mach number correction and the angle of attack increment, to obtain these two parameters and $\left(\frac{C_{L,max}}{c_{lmax}}\right)$ the reader should refer to the curves in DATCOM (Hoak & Carlson, 1978).

However, the use of DATCOM equations employed a hybrid approach. For the zero-lift angle of attack, $\boldsymbol{\alpha_0}$, and lift curve slope, $\boldsymbol{C_{L\alpha}}$, the VSPAERO solver is used. In contrast, the airfoil's maximum lift coefficient, $\boldsymbol{c_{lmax}}$, is determined from XFOIL.

The model was validated by comparing its results to those of the CFD of the wing. As it shows in Fig. 10, there are two main regions: linear and nonlinear.

- For the linear region where the angle of attack goes from -2° to 8.5°, the curves present a close result with the same value of the curve slope (0.0889 1/°). It is remarkable; there is a little difference in the lift coefficient at zero angle between CFD and framework results, which is equal to 0.24 and 0.28, respectively.
- For the nonlinear zone, it is observed that the proposed code models the stall and pre-stall effects. $C_{L,max}$ for the suggested method was 1.41 at a stall angle of 14.8°, whereas 1.34 was the value estimated by CFD at a stall angle of 15.5°. Hence, it can be observed that there is no greater than 5.3% absolute error between the proposed approach and the CFD results in $C_{L,max}$ estimation.

5. COMPARATIVE ANALYSIS AND VALIDATION OF THE FRAMEWORK OPTIMIZATION

The proposed framework was installed on a personal computer with an i7-8750H-2.20GHz CPU processor and 16 GB of RAM. In order to test the validation of the code. The validation of the framework optimization was compared to the reference study. Where they seek to maximize endurance ($\frac{{C_L}^{\frac{3}{2}}}{C_D}$) using a combination of an artificial neutral network and XFLR5 software.

5.1 Problem Definition and Constraints

The goal is to optimize the endurance ratio (${C_L}^{3/2}/C_D$), hence, the objective function to be maximized is:

$f = -\frac{{C_L}^{\frac{3}{2}}}{C_D} + T$, where T represents the constraint's penalty term, it can be expressed by the following formulation:

Table 4 Domain of experiment

Design variables	Lower Bound	Upper Bound
$W_l\ [kg/m^2]$	8	10
λ	0.55	0.83
A	8	11
$\theta\ [\circ]$	-5	0

$$T = max(0, V_s(t) - V_s{}^*)^2 + max\left(0, ROC^* - ROC(t)\right)^2 + max\ (0, V_{max}{}^* - V_{max}(t))^2 \quad (18)$$

Here: $ROC^*, V_s{}^*, V_{max}{}^*$ represent the required performance. To ensure a fair comparison with the reference study, we employed the same propeller model used in that study for performance evaluation.

$t\ =\ [\ A,\ W_l,\ \lambda,\ \theta]$: is the design vector.

The problem can be expressed in the following way:

$$Minimize\ f(t) =\ Min\ (-\frac{C_L{}^{\frac{3}{2}}}{C_D} + T) \quad (19)$$

Subject to:

- $ROC(t)\ \geq\ 5\ m/s$
- $V_{max}\ (t)\ \geq\ 100\ km/h$
- $V_s\ (t)\ \ \leq\ 10\ m/s$

The design variables in this problem are: Wing loading (W_l), Aspect Ratio (A), Taper Ratio (λ) and Twist Angle (θ), the test domain is expressed in Table 4 .

5.2 Framework Parametrization

The study framework consists of various aerodynamic inputs and parameters related to the genetic algorithm. The aerodynamic parameters include the Mach number, which is fixed at zero, and the angle of attack, which is selected within an interval that could capture the maximum endurance coefficient. The side slip angle is set to zero in this study and the weight of the UAV. Additionally, the number of tessellated curves in the spanwise direction (Num W) is set at 33, while the number of tessellated curves in the cord direction (Num U) is set at 30. These last two values are fixed after following the convergence of the lift and drag coefficients at zero incidence as a function of the number of panels, as in Fig. 11 and Fig. 12.

At first, the house code was launched for 10 generations and a population that contained only 10 chromosomes; then, it was launched for a population of 20 and 30 chromosomes to allow for more exploration of the field research. The time simulation is proportional to the number of chromosomes in the population; it takes, on average, 46 minutes for N-pop = 10, 88 minutes for N-pop = 20, and 172 minutes for N-pop = 30 chromosomes. The first generation was generated arbitrarily according to the value of each variable listed in the table above. The percentages of selection, elitism, and crossover operations

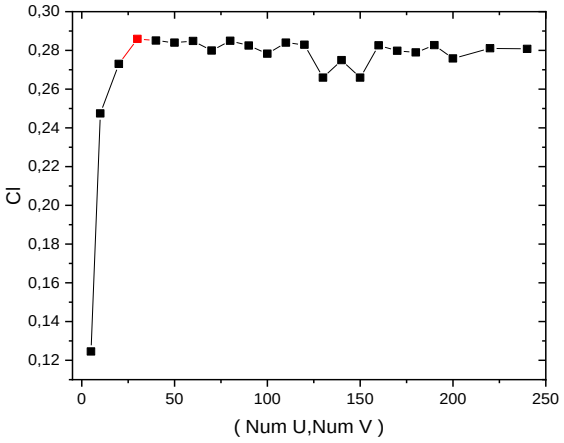

Fig. 11 C_L convergence vs. number of tessellations

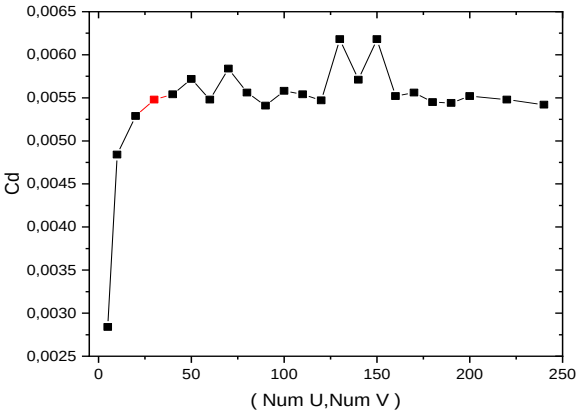

Fig. 12 C_D convergence vs. number of tessellations

used in the genetics algorithm are, respectively, 30%, 40%, and 30%. It is noticed that a limiter is used to ensure that the generation of arbitrary gens adheres to the lower and upper boundaries of the domain of experiment.

5.3 Optimization Results

After getting the different geometry dimensions using OpenVSP-API, their performances were compared to the geometry obtained using ANN-XFLR5 (reference study). XFLR5 software version 6.48 simulates each geometry. The 3D panel method was chosen with panel elements equal to 4970.

Figure 13 presents the evolution of $\left(\frac{CL^{\frac{3}{2}}}{C_D}\right)$ in function of angle of attack. Notably, both the proposed ANN-XFLR5 and OpenVSP-API optimization methods yield similar results for both planform wing size and endurance coefficient. It is observed that all wings exhibit a region of gentle variation over the maximum value of endurance that ensures good endurance for an important range of angles of attack. Furthermore, the maximum endurance ratio is increased from 23.91 using ANN-XFLR5 optimization to 24.29, 24.22, and 24.36 using OpenVSP-API with N-pop values of 10, 20, and 30 respectively. These graphs demonstrate that applying the research framework can increase endurance by up to 1.88%. The

Table 5 Optimized wing shapes and their performance

	W_l [kg/m^2]	A	λ	θ [deg]	b [m]	C_t [m]	C_r [m]	E_{max}	**Time** [min]
ANN-XFL5	8.6	10.51	0.55	0	2.929	0.198	0.359	23.91	x
OpenVSP-API (N-pop=10)	8.9	10.87	0.64	-0.09	2.919	0.209	0.328	24.29	46
OpenVSP-API (N-pop=20)	8.9	10.84	0.78	-0.06	2.914	0.235	0.303	24.22	88
OpenVSP-API (N-pop=30)	9.0	10.98	0.69	-0.20	2.921	0.217	0.315	24.36	172

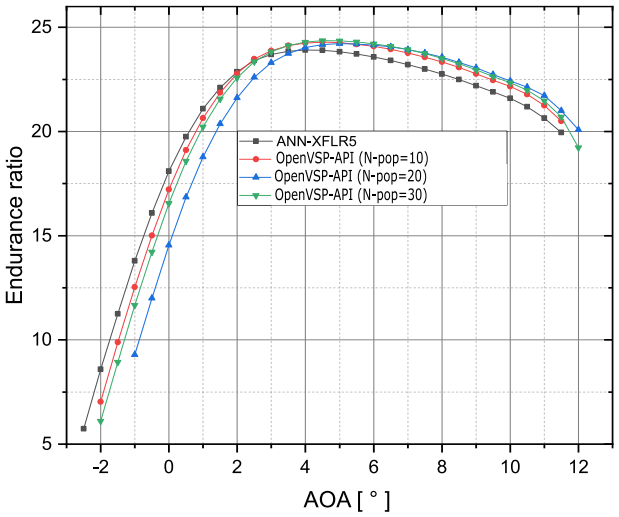

Fig. 13 Endurance ratio vs. angle of attack

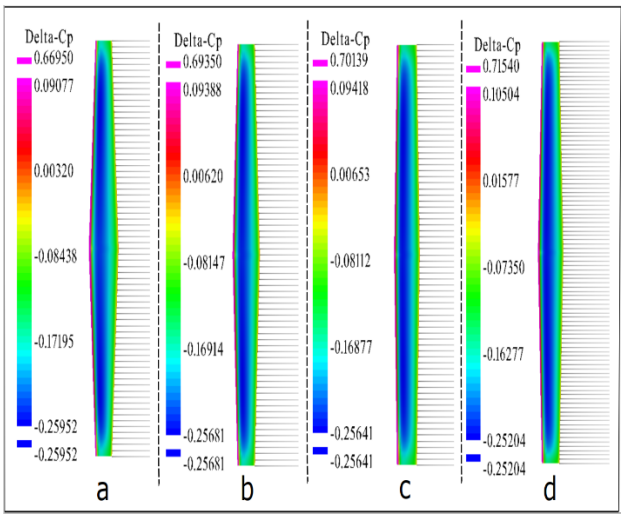

Fig. 14 Pressure distribution over wings

geometry parameters are represented in Table 5 The improvement in endurance ratio is explained by the increment in the aspect ratio from 10.51 to 10.98 using ANN-XFLR5 and OpenVSP-API, respectively. Furthermore, it has been highlighted that with a decreasing taper ratio among wings at low incidence angles, there is an increase in endurance. This is attributed to the reduction in induced drag associated with the decrease in the taper ratio.

Figure 14 shows the pressure distribution at zero angle of attack on the four wing shapes obtained, respectively, by: a) ANN-XFLR5, b) OpenVSP-API (N-pop = 10), c) OpenVSP-API (N-pop = 20), and d) OpenVSP-API (N-pop = 30). Overall, a similarity is observed in the distribution of pressure between wings obtained either by ANN-XFLR5 or by the OpenVSP-API framework. However, it is noticeable that there is a suppression area over the leading edge of the wings obtained by OpenVSP-API compared to ANN-XFLR5.

6. CFD ANALYSIS

6.1 Governing Equations

The CFD study was performed using the commercial software Ansys Fluent (Ansys Fluent 2023). The coupled Reynolds-Averaged Navier-Stokes (RANS) equations of continuity, momentum, and energy, shown in Equations 20, 21, and 22 (Katz & Plotkin, 2001), were solved alongside the Spalart-Allmaras turbulence model.

Continuity equation:

$$\frac{\partial \rho}{\partial t} + \nabla \cdot \left(\rho \vec{V}\right) = 0 \tag{20}$$

Momentum equation:

$$\frac{\partial \left(\rho \vec{V}\right)}{\partial \mathrm{t}} + \nabla \cdot \left(\rho \vec{V}\,\vec{V}\right) = -\nabla p + \rho \vec{f} + \nabla \cdot \tau \tag{21}$$

Energy equation:

$$\rho \frac{D}{Dt}\left(e_i + \frac{1}{2}V^2\right) = \nabla \cdot \left(p\vec{V}\right) - \nabla \cdot \vec{q} + \rho \vec{f} \cdot \vec{V} \tag{22}$$

The general equation of the Spalart-Allmaras turbulence model represented in Equation 24 (Singh et al., 2021):

$$\frac{D(\tilde{v})}{Dt} = \text{production} + \text{diffusion} - \text{dissipation} \tag{24}$$

Where $\tilde{v}$ represents the turbulent viscosity.

6.2 Computational Domain and Grid Generation

The computational domain for the simulations is depicted in Fig. 15. An unstructured mesh, consisting of $2.7 \cdot 10^6$ nodes and $7.3 \cdot 10^6$ elements, was generated as shown in Fig. 15. This number of nodes was found by an investigation of the dependency between the number of nodes and the results. Furthermore, 15 inflation layers are created, the first of which is positioned $1.8 \cdot 10^{-5}$ m from the wall and provides a value for the non-dimensional wall distance (y+) remained below 1.

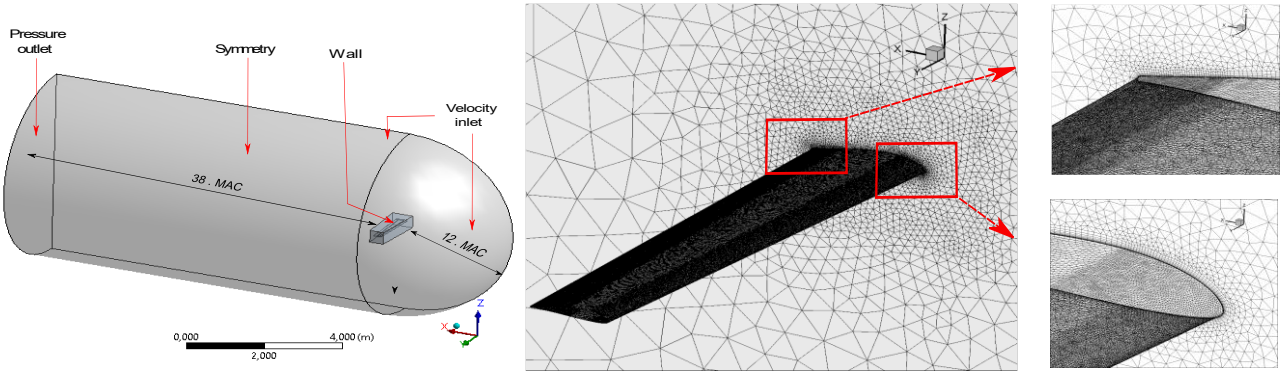

Fig. 15 Calculation domain and grid generation for CFD

Table 6 Boundary condition

Zone	Type	Boundary condition
Inlet	Velocity inlet	Magnitude velocity =17 m/s Inlet pressure = 97851 Pa Temperature =286.2 k
Outlet	Pressure outlet	Outlet pressure = 97851 Pa Temperature =286.2 k
Symmetry	Symmetry	
Wing	Wall	Stationary wall, Condition of no-slip

Table 7 solver setup and solution methods

solver	Pressure based
Pressure-Velocity coupling	Coupled
Formulation	Implicit
Discretization method	2nd order upwind
Turbulence model	Spalart-Allmaras
Gradient	Least squares cell based
Residual: continuity, velocity, nut	10^{-5}
Initialization	Hybrid

6.3 Boundary Conditions

Figure 15 illustrates the boundary conditions. a velocity of 17 m/s at the inlet, which corresponds to a Reynolds number of $3.0 \cdot 10^5$ based on the MAC). Ambient pressure at the outlet, and a symmetry condition applied to one-half of the wing to reduce computational time. Additionally, all wing surfaces were assigned as walls with zero velocity. Table 6 provides the detailed boundary conditions specified for each zone.

6.3 Solver Setup

Ansys Fluent was used to simulate the wing produced by an optimization process utilizing the internal research house code, with a population of 30 chromosomes ranging from -2 to 16° angles of attack. In the present study, the flow is incompressible. Therefore, a pressure-based solver has been chosen. Additionally, a coupled solver has been selected to resolve the momentum and pressure equations simultaneously. Table 7 summarizes the solver parameters and solution methods.

Figure 16 displays the aerodynamic properties of the optimized wing, generated with the OpenVSP-API for a population of 30 chromosomes. The XFLR5 (3D panel) and OpenVSP (VLM) yield maximum L/D values of 29.6 and 56, respectively, while OpenVSP-API achieves a value of 20.2, which is relatively close to the CFD (21.1) value. The non-modeling of the viscous effect in OpenVSP and XFLR5 leads to the prediction of low drag levels by both the VLM and 3D panel methods. Both OpenVSP-API and CFD have the capability to calculate $C_{L,max}$ values of 1.381 and 1.415, respectively, at an angle of attack of 13.8° and 13°. It is observed that the absolute error in estimating $C_{L,max}$ reduces to 2.4% in this scenario.

Figure 17 shows the streamlines and static pressure distribution over the wing. This may be quite helpful for locating the flight control surfaces and determining the region of separation. Additionally, by understanding the pressure distribution throughout the wing, the weak points in the structure that require reinforcement can be identified relative to others, which will aid in structural optimization later on.

Figure 18 shows the line speed of the magnitude velocity over the root profile. It is observed that the more the angle of attack increases, the separation of the flow begins with the trailing edge and will create what is called the Laminar Separation Bubble (LSB) and enlarges and shifts towards the leading edge.

7. CONCLUSION

A novel framework for aerodynamic preliminary sizing of mini-UAVs has been developed, prioritizing the maximization of flight endurance which a critical factor for achieving mission objectives in surveillance applications. This framework leverages a calibrated aerodynamic solver that utilizes the Vortex Lattice Method (VLM) to estimate linear lift, induced drag, and incorporates a semi-empirical parasite drag model based on friction coefficient and form factor. Additionally, an estimation of maximum lift coefficient and stall angle is introduced through the adaptation of the DATCOM method. The framework employs Python scripts to call VSPAERO for VLM computation, the Parasite Drag tool for estimating C_{D0}, XFOIL, and the DATCOM method for stall prediction.

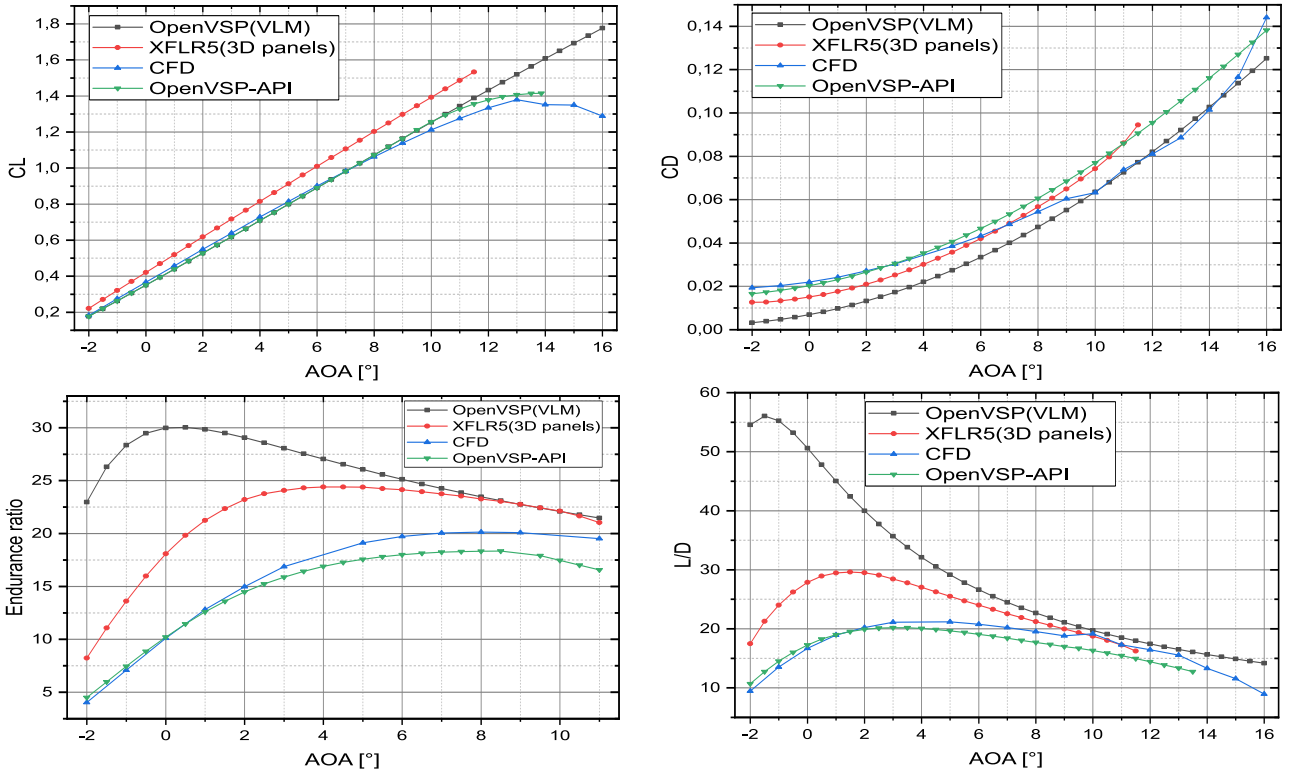

Fig. 16 Aerodynamic performances of the ideal wing

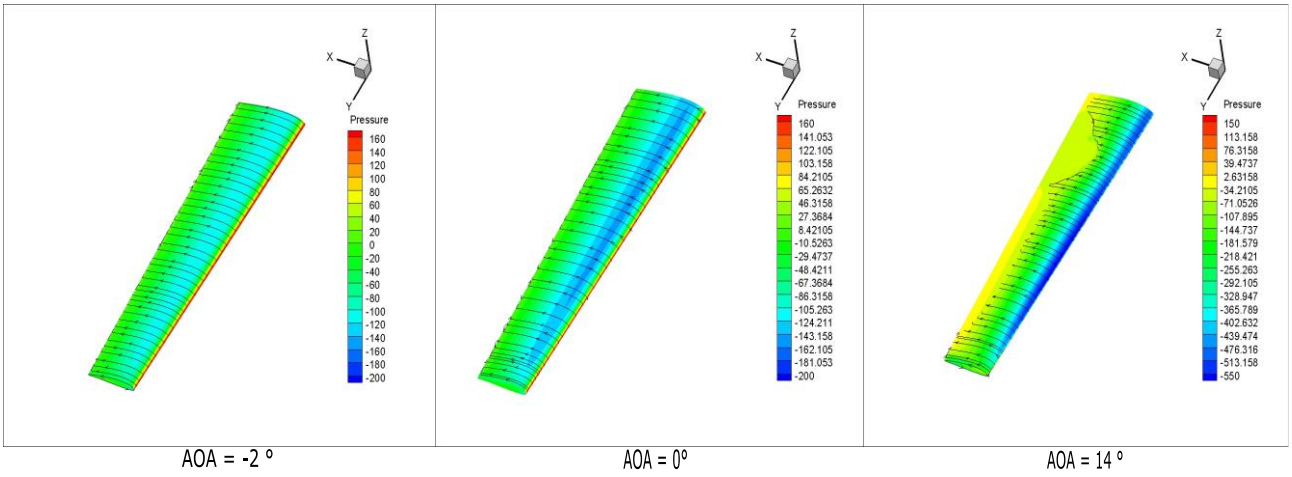

Fig. 17 Pressure distribution over the optimal wing

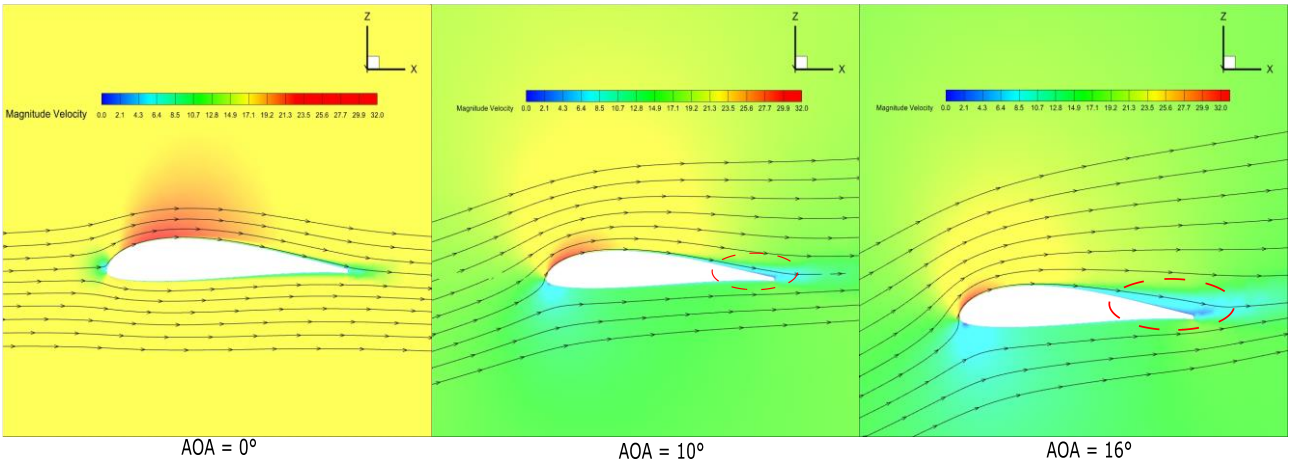

Fig. 18 Line speed of the magnitude velocity over the root profile

The results generated by the adopted aerodynamic solver are compared to those from a reference study, exhibiting promising agreement and behavior. Such a solver reduces the gap for both drag and lift, referred to CFD results.

To test the constructed tool, a wing design was carried out to meet a set of desired requirements. The process involved weight estimation, profile selection, design point determination, and GA aerodynamic optimization. The obtained results indicate that the elaborated framework provides promising solutions for wing dimensions and performances. In comparison to the reference study (ANN-XFLR5), our automated process allows for simulations at various angles of attack and flight conditions, eliminating the need for big data.

The utilization of this framework offers a systematic, fast, and efficient tool for designing, analyzing, and optimizing UAV wings.

ACKNOWLEDGEMENT

A part of this investigation was conducted at the Department of Automotive and Aeronautical Engineering at Hamburg University of Applied Sciences. The authors express their gratitude to the staff at HAW Hamburg for providing a conducive environment for academic growth and collaboration throughout the research process. Additionally, we extend our thanks to the IMLET Institute for their meticulous language editing and proofreading.

CONFLICT OF INTEREST

The author declares that there is no conflict of financial or non-financial interest to disclose.

AUTHORS CONTRIBUTION

M. Sahraoui: Data curation, Investigation, Software, Visualization, Formal analysis, Writing – original draft; **A. Boutemedjet**: Data curation, Resources, Methodology, Visualization, Software; **M. Mekadem**: Visualization, Supervision, Writing – review & editing; **D. Scholz**: Methodology, Writing – review & editing.

REFERENCES

OpenVSP. (2023, July 24). Open Vehicle Sketch Pad (Version 3.25.0). https://openvsp.org

Air Force Technology | Air Defence News & Views Updated Daily. (2024, February 2). Airforce Technology. https://www.airforce-technology.com

Ansys CFX. (2023, October 3). Industry-Leading CFD Software. https://www.ansys.com/products/fluids/ansys-cfx

Ansys Fluent. (2023, October 3). Fluid Simulation Software. https://www.ansys.com/products/fluids/ansys-fluent

Anderson, J. D. (2016). *Introduction to flight* (Eighth edition). McGraw-Hill Education.

Anılır, B., & Kurtuluş, D. F. (2023). Unsteady aerodynamic performance of SD7062 airfoil at high Reynolds number. *Progress in Computational Fluid Dynamics, An International Journal*, *23*(2), 65. https://doi.org/10.1504/PCFD.2023.129760

Azabi, Y., Savvaris, A., & Kipouros, T. (2019). Artificial intelligence to enhance aerodynamic shape optimisation of the aegis UAV. *Machine Learning and Knowledge Extraction*, *1*(2), 552–574. https://doi.org/10.3390/make1020033

Bahrami, A., Hoseinzadeh, S., Heyns, P. S., & Mirhosseini, S. M. (2019). Experimental investigation of co-flow jet's airfoil flow control by hot wire anemometer. *Review of Scientific Instruments*, *90*(12), 125107. https://doi.org/10.1063/1.5113592

Benaouali, A., & Kachel, S. (2019). Multidisciplinary design optimization of aircraft wing using commercial software integration. *Aerospace Science and Technology*, *92*, 766–776. https://doi.org/10.1016/j.ast.2019.06.040

Blasius, H. (1950). *The boundary layers in fluids with little friction*. National Advisory Committee for Aeronautics.

Boutemedjet, A., Samardžić, M., Rebhi, L., Rajić, Z., & Mouada, T. (2019). UAV aerodynamic design involving genetic algorithm and artificial neural network for wing preliminary computation. *Aerospace Science and Technology*, *84*, 464–483. https://doi.org/10.1016/j.ast.2018.09.043

Cheeseman, I. (1976). Fluid-Dynamic Drag: Practical Information on Aerodynamic Drag and Hydrodynamic Resistance. SF Hoerner. Hoerner Fluid Dynamics, Brick Town, New Jersey. 1965. 455 pp. Illustrated. $24.20. *The Aeronautical Journal*, *80*(788), 371–371.

Covert, E. E. (1985). *Progress in astronautics and aeronautics: Thrust and drag: Its prediction and verification* (Vol. 98). AIAA.

dos Santos, C. R., & Marques, F. D. (2018). Lift prediction including stall, using vortex lattice method with Kirchhoff-based correction. *Journal of Aircraft*, *55*(2), 887–891. https://doi.org/10.2514/1.C034451

Du, X., He, P., & Martins, J. R. R. A. (2021). Rapid airfoil design optimization via neural networks-based parameterization and surrogate modeling. *Aerospace Science and Technology*, *113*, 106701. https://doi.org/10.1016/j.ast.2021.106701

Elham, A., & Van Tooren, M. J. L. (2014). Winglet multi-objective shape optimization. *Aerospace Science and Technology*, *37*, 93–109. https://doi.org/10.1016/j.ast.2014.05.011

Falkner, V. M. (1943). *The calculation of aerodynamic loading on surfaces of any shape*.

Gudmundsson, S. (2013). *General aviation aircraft design: Applied Methods and Procedures*. Butterworth-Heinemann.

Haryanto, I., Utomo, T. S., Sinaga, N., Rosalia, C. A., & Putra, A. P. (2014). Optimization of maximum lift to drag ratio on airfoil design based on artificial neural network utilizing genetic algorithm. *Applied Mechanics and Materials*, *493*, 123–128. https://doi.org/10.4028/www.scientific.net/AMM.493.123

Hedman, S. G. (1966). *Vortex lattice method for calculation of quasi steady state loadings on thin elastic wings in subsonic flow* (p. 0018).

Hoak, D.E., and Carlson, J. (1978). *USAF Stability and Control DATCOM*, Air Force Flight Dynamics Laboratory.

Hoseinzadeh, S., Bahrami, A., Mirhosseini, S. M., Sohani, A., & Heyns, S. (2020). A detailed experimental airfoil performance investigation using an equipped wind tunnel. *Flow Measurement and Instrumentation*, *72*, 101717. https://doi.org/10.1016/j.flowmeasinst.2020.101717

Hoseinzadeh, S., Sohani, A., & Heyns, S. (2021). Comprehensive analysis of the effect of air injection on the wake development of an airfoil. *Ocean Engineering*, *220*, 108455. https://doi.org/10.1016/j.oceaneng.2020.108455

Hoseinzadeh, S., & Stephan Heyns, P. (2022). Development of a model efficiency improvement for the designing of feedwater heaters network in thermal power plants. *Journal of Energy Resources Technology*, *144*(7), 072102. https://doi.org/10.1115/1.4054196

Hutagalung, M. R. A., Latif, A. A., & Israr, H. A. (2016). Structural design of UAV semi-monoque composite wing. *Journal of Transport System Engineering*, 26-34.

Kapsalis, S., Panagiotou, P., & Yakinthos, K. (2021). CFD-aided optimization of a tactical blended-wing-body UAV platform using the taguchi method. *Aerospace Science and Technology*, *108*, 106395. https://doi.org/10.1016/j.ast.2020.106395

Katz, J., & Plotkin, A. (2001). *Low-speed aerodynamics*. (Vol. 13), Cambridge university press.

Masood, K., & Wei, Z. (2018). Robust multidisciplinary optimization for wing of a low subsonic UAV. *Journal of Biodiversity & Endangered Species*, *09*(02). https://doi.org/10.4172/2332-2543.1000226

Ostadhossein, R., & Hoseinzadeh, S. (2024). Developing computational methods of heat flow using bioheat equation enhancing skin thermal modeling efficiency. *International Journal of Numerical Methods for Heat & Fluid Flow*, *34*(3), 1380–1398. https://doi.org/10.1108/HFF-06-2023-0355

Pritchard, P. J., & Mitchell, J. W. (2016). *Fox and McDonald's introduction to fluid mechanics*. John Wiley & Sons.

Sadraey, M. H. (2013). *Aircraft design: A systems engineering approach*. Wiley.

Schlichting, H., & Kestin, J. (1961). *Boundary layer theory* (Vol. 121). Springer.

Singh, D. K., Jain, A., & Paul, A. R. (2021). Active flow control over a naca23012 airfoil using hybrid jet. *Defence Science Journal*, *71*(6), 721–729. https://doi.org/10.14429/dsj.71.16468

Sun, G., & Wang, S. (2019). A review of the artificial neural network surrogate modeling in aerodynamic design. *Proceedings of the Institution of Mechanical Engineers, Part G: Journal of Aerospace Engineering*, *233*(16), 5863–5872. https://doi.org/10.1177/0954410019864485

Traub, L. W. (2013). Aerodynamic impact of aspect ratio at low reynolds number. *Journal of Aircraft*, *50*(2), 626–634. https://doi.org/10.2514/1.C031980